Nuclear Engineering and Technology 54 (2022) 2840–2851

Contents lists available at ScienceDirect

Nuclear Engineering and Technology

journal homepage: www.elsevier.com/locate/net

Original Article

Operation optimization of auxiliary electric boiler system in HTR-PM nuclear power plant

Xingxuan Du [a], Xiaolong Ma [b], Junfeng Liu [b, c], Shifa Wu [c], Pengfei Wang [c, *]

[a] School of Management, Xi'an University of Architecture and Technology, Xi'an, 710055, Shaanxi, China
[b] Xi'an Thermal Power Research Institute Co. Ltd, Xi'an City, 710054, China
[c] Shaanxi Key Laboratory of Advanced Nuclear Energy and Technology, And Shaanxi Engineering Research Center of Advanced Nuclear Energy, Xi'an Jiaotong University, Xi'an, 710049, China

ARTICLE INFO

Article history:
Received 10 January 2022
Received in revised form
4 February 2022
Accepted 16 February 2022
Available online 18 February 2022

Keywords:
Electric boiler
Hot standby
Operation optimization
Transient response speed
Power consumption

ABSTRACT

Electric boilers (EBs) are the backup steam source for the auxiliary steam system of high-temperature gas-cooled reactor nuclear power plants. When the plant is in normal operations, the EB is always in hot standby status. However, the current hot standby operation strategy has problems of slow response, high power consumption, and long operation time. To solve these problems, this study focuses on the optimization of hot standby operations for the EB system. First, mathematical models of an electrode immersion EB and its accompanying deaerator were established. Then, a control simulation platform of the EB system was developed in MATLAB/Simulink implementing the established mathematical models and corresponding control systems. Finally, two optimization strategies for the EB hot standby operation were proposed, followed by dynamic simulations of the EB system transient from hot standby to normal operations. The results indicate that the proposed optimization strategies can significantly speed up the transient response of the EB system from hot standby to normal operations and reduce the power consumption in hot standby operations, improving the dynamic performance and economy of the system.

1. Introduction

High-temperature gas-cooled reactors (HTGRs) are the reactors that use gas as coolant and have the advantages of inherent safety, high power generation efficiency, good economics, and versatility [1–3], which are rated as one of the most promising Generation IV reactors by the Generation IV International Forum [4]. Owing to the high outlet coolant temperature of HTGRs (750°C–900 °C), they have the prospect of comprehensive applications, such as hydrogen production from nuclear energy and nuclear energy for heating. Therefore, HTGRs have important research significance and application prospects for reducing carbon emissions and achieving carbon peaking and carbon neutrality goals. Currently, many countries around the world are interested in the research and development of HTGRs and have made significant efforts [5–8].

The High Temperature Reactor-Pebble bed Module (HTR-PM) [9,10] is a Generation IV reactor technology developed independently by China. The Shidao Bay nuclear power plant (NPP) demonstration project using HTR-PM technology was first connected to the grid on December 20, 2021. In the absence of supply conditions for turbine steam extraction, the HTR-PM NPP requires an auxiliary boiler to provide heating steam which enters the deaerator to heat the feedwater and meet the required temperature of the steam generator feedwater. During the start-up and shutdown phases of the HTR-PM NPP, the auxiliary boiler provides qualified steam to the user of the auxiliary steam system, who will depressurize the steam for further use.

The auxiliary boiler used for auxiliary steam supply in NPPs can be the coal-fired, oil-fired, and electric boilers. In actual engineering practice, the auxiliary boiler should be selected according to the operating characteristics and requirements of the target NPP. Compared with conventional pressurized water reactor (PWR) NPPs, HTGR NPPs have the following characteristics. On the one hand, there is a fundamental difference in steam parameters between HTGR and PWR NPPs. The turbine inlet steam of PWR plants is saturated steam, and the required steam temperature for the turbine shaft seal system is low. Moreover, the large water volume in the PWR steam generator can provide saturated steam for its

* Corresponding author.
E-mail address: wangpengfei@xjtu.edu.cn (P. Wang).

https://doi.org/10.1016/j.net.2022.02.015

turbine shaft seal system for a long time after the turbine trip, while the turbine inlet steam of the HTGR NPP is superheated steam (566 °C for HTR-PM NPP). Its turbine shaft seal system requires steam with higher temperature (380 °C), and there is no reliable standby steam source in the plant after the turbine trip. Therefore, the auxiliary boiler that can provide qualified auxiliary steam is highly demanded. Moreover, the auxiliary boiler needs to be started as soon as possible to avoid cold gas entering the turbine. On the other hand, HTGR NPPs have higher feedwater quality requirements than PWR NPPs. Compared with the conventional coal-fired and oil-fired boilers, electric boilers (EBs) have many advantages, such as fast start-shutdown speed, high control accuracy, convenient operation and maintenance, high energy efficiency, low carbon emission, and environmental protection. They have long replaced the early coal-fired and oil-fired boilers in the design and selection of backup steam sources for auxiliary steam systems in NPPs. The electrode injection-type EBs are being replaced by the electrode immersion-type EBs recently. Therefore, through the comparison of different types of EBs and also considering the higher feedwater and steam quality requirements, the electrode immersion-type EB is chosen for the HTR-PM NPP.

Currently, there are many studies focusing on the mathematical modeling, dynamic simulation, and control studies of various types of NPPs under normal operating conditions [11–14], including the HTR-PM NPP [15–17]. While few have been conducted on the operation and control strategies of the auxiliary boiler systems under special operating conditions such as test run, start-up, and shutdown. Actually, during the engineering construction of the HTR-PM NPP in China, some shortcomings in the operation strategy of the current EB system have been identified, as illustrated below. First, the EB system needs to run for a long time during the test run, start-up, and shutdown operations of the HTR-PM NPP. Moreover, the NPP needs auxiliary steam to heat the steam generator feedwater after a sudden trip of the turbine. Therefore, the EB providing auxiliary steam must be in hot standby operation even during normal operations of the NPP. However, according to the current hot standby operation strategy, the EB consumes considerable electric power to compensate for its heat loss to the environment and cannot provide qualified heating steam in a short period of time. It takes a long time to change from the hot standby operation to the normal operation, which poses a hidden risk for the safe operation of the NPP. Therefore, the optimization of the EB hot standby operation strategy is of great important for the safe and economic operations of the HTR-PM NPP.

In view of the above, this study proposed optimization strategies for the EB hot standby operation to address the existing problems, the feasibility and superiority of which were verified by simulation. This remainder of paper is organized as follows. Section 2 presents the mathematical modeling of the EB system compromising an electrode immersion-type EB and a build-in thermal deaerator. The operating characteristics and control systems of the EB system are introduced in Section 3, followed by the illustration of proposed optimization strategies in Section 4. Verification of these strategies through numerical simulations are present in Section 5 with the results discussed. Conclusions are drawn in Section 5.

2. Mathematical modeling of EB system

2.1. System description

The auxiliary steam during start-up and shutdown of the HTR-PM NPP is provided by the auxiliary EB system. It is designed to supply 35 t/h of steam with rated parameters of 1.25 MPa and 193.4 °C for auxiliary steam system and also provide 4 t/h steam that is further heated by a superheater to 215–350 °C for the turbine shaft seal system. The EB system consists of a high-voltage electrode immersion-type EB, a deaerator, a steam superheater, and other auxiliary feedwater devices.

The EB adopts inner and outer cylinder structure, mainly composed of the inner cylinder, outer cylinder, three-phase electrode, circulation pump, and feedwater pump, as shown in Fig. 1. The inner cylinder of the EB is the equipment for generating steam, and the three-phase electrodes are submerged in the furnace water with a certain electrical conductivity, which is used to generate steam by heating the furnace water with voltage. The EB replenishes the water in the inner cylinder through the circulation pump, and the high conductivity water is discharged to the outer cylinder through the inner cylinder drain valve. The inner cylinder water level is controlled to regulate the EB power. The deviation of the EB power from its setpoint value is used to adjust the circulation pump of the inner cylinder to maintain its water level.

The deaerator of the HTR-PM EB system is a built-in thermal deaerator which can supply a rated feedwater flow rate of 100 t/h and a maximum feedwater flow rate of 200 t/h for the EB. The rated operating pressure and temperature of the deaerator are 0.12 MPa and 105 °C, respectively. The deaerator is mainly used to remove waste gas (mainly oxygen) from the inlet feedwater and preheat the feedwater to reduce the thermal stress in the feedwater pipes connected with the EB. The deaerator removes the dissolved gas from the inlet feedwater by atomizing it through a nozzle.

In summary, the EB system of the HTR-PM NPP has the following main functions.

(1) It can provide qualified steam to the secondary loop auxiliary steam header during the start-up and shutdown of the plant.
(2) It supplies heating steam to the turbine shaft seal system during the start-up of the plant.
(3) When the plant is in normal operations, it is in hot standby status.
(4) It provides reliable steam for the turbine shaft seal system and auxiliary steam header when other steam sources cannot meet the requirements.
(5) During load rejection transients of the plant, the heating steam pumped to the secondary loop deaerator is

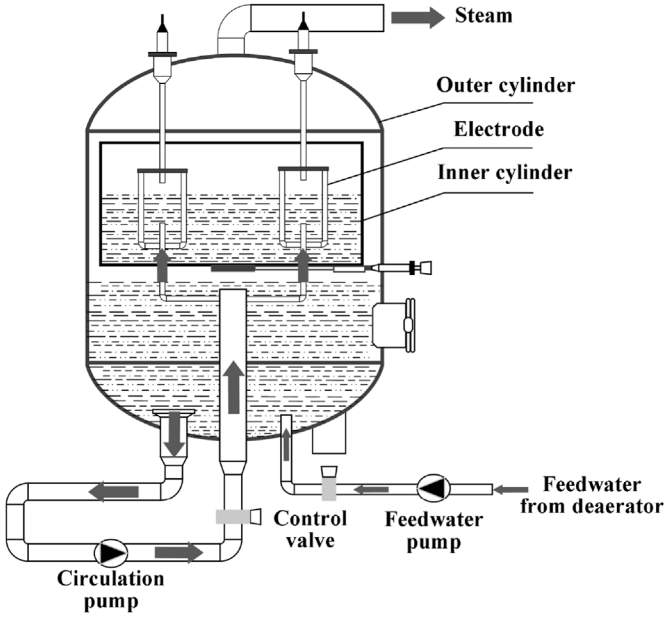

Fig. 1. Schematic of the electrode immersion-type EB.

interrupted. In this case, the EB system can start quickly to supply heating steam to the deaerator to maintain the feedwater temperature and reduce the thermal shock to the steam generator.

2.2. EB model

The structure and operating principle of the EB in this study are schematically shown in Fig. 1. In the mathematical modeling, the EB can be physically structured into the inner cylinder water, outer cylinder water, and steam regions. Thus, a non-equilibrium three-region EB model can be developed based on basic conservation laws of mass, energy, and volume.

2.2.1. Physical model

During transient processes, the steam in the EB steam region can be superheated steam, saturated steam, or vapor-water mixture. While the water in the water regions of the inner and outer cylinders can be subcooled water, saturated water, or vapor-water mixture. During transient operations, various thermal phenomena may occur in the EB. The modeling processes of the thermal phenomena are given as follows.

2.2.1.1. Bubble rising in the water region. During the transient process of pressure decrease, the subcooled water in the EB tends to saturate. When the subcooled water reaches saturation, bubbles are generated in the inner and outer cylinder water regions and rise to the steam region. The flow rate of bubbles escaping from the water regions can be calculated by [18].

$$W_{be}=\begin{cases}0 & h_l \le h_f \\ \alpha_L A V_{bub}\rho_g & h_f < h_l < h_g\end{cases} \tag{1}$$

where W_{be} is the bulk evaporation flowrate, kg/s; A is the cross-section area of the water region, m^2; V_{bub} is the bubble rise velocity, m/s; ρ_g is the saturated steam density, kg/m^3; h_l is water enthalpy, kJ/kg; h_f and h_g are the enthalpies of saturated water and steam, respectively, kJ/kg; α_L is the void fraction in the water region, which can be calculated by

$$\alpha_L=\frac{x_L v_g}{x_L v_g+(1-x_L)v_f} \tag{2}$$

$$x_L=\frac{h_l-h_f}{h_g-h_f} \tag{3}$$

here, x_L denotes the vapor content in the water region of the EB.

The bubble rising velocity can be determined by the Wilson's formula as [19].

$$V_{bub}=\max(V_{b1},V_{b2}) \tag{4}$$

$$V_{b1}=\left(\frac{\alpha}{0.136}\right)^{0.5168}\left(\frac{\rho_f-\rho_g}{\rho_g}\right)^{0.1798}\left(d\Big/\sqrt{\frac{\sigma}{\rho_f-\rho_g}}\right)^{0.1067}\left(g\sqrt{\frac{\sigma}{\rho_f-\rho_g}}\right)^{0.5} \tag{5}$$

$$V_{b2}=\left(\frac{\alpha}{0.75}\right)^{1.333}\left(\frac{\rho_f-\rho_g}{\rho_g}\right)^{0.4267}\left(d\Big/\sqrt{\frac{\sigma}{\rho_f-\rho_g}}\right)^{0.2533}\left(g\sqrt{\frac{\sigma}{\rho_f-\rho_g}}\right)^{0.5} \tag{6}$$

where σ is the surface tension of water, N/m; v_f and v_g are the specific volumes of saturated water and steam, respectively, kJ/kg.

2.2.1.2. Rain-out in the steam region. During transient processes, the condensate droplets in the steam region will fall to the water regions when the superheated steam reaches saturation. The steam condensation flow rate can be calculated by [18].

$$W_{bc}=\begin{cases}0 & h_v \ge h_g \\ (1-\alpha_v)A\rho_f V_d & h_f < h_v < h_g\end{cases} \tag{7}$$

where V_d is the liquid droplet velocity at the steam-water interface which can be given as a constant, m/s; ρ_f is the saturated water density, kg/m^3; h_v is the steam enthalpy in the steam region, kJ/kg; α_v is the void fraction of the steam region, which can be calculated by

$$\alpha_v=\frac{x_v v_g}{x_v v_g+(1-x_v)v_f} \tag{8}$$

$$x_v=\frac{h_v-h_f}{h_g-h_f} \tag{9}$$

here, x_v denotes the steam quality in the EB.

2.2.1.3. Wall condensation. The condensation flowrate of steam on the EB wall can be expressed as

$$W_{cw}=\frac{Q_{cw}}{h_v-h_f} \tag{10}$$

where W_{cw} is the steam condensation flowrate on the wall, kg/s; Q_{cw} is the condensation heat transfer quantity, kW, which can be calculated by

$$Q_{cw}=K_{cw}A_{cw}(T_v-T_w) \tag{11}$$

where K_{cw} is heat transfer coefficient between the steam and wall

in the steam region, kW/(m^2·K); A_{cw} is heat transfer area between the steam and wall in the steam region, m^2; T_v is the steam temperature, °C; T_w is the wall temperature, °C.

According to the Nusselt equation for membrane condensation on vertical walls, the heat transfer coefficient between the steam and wall can be expressed as [20].

$$K_{cw} = 1.13\left[\frac{g\rho^2\lambda^3 r}{\eta(T_v - T_w)L_{cw}}\right]^{1/4} \tag{12}$$

where L_{cw} is the height of the wall in the steam region, m; ρ, λ, and η are the density (kg/m^3), thermal conductivity (W·m^{-1}·K^{-1}), and dynamic viscosity (N·s·m^{-2}) of the condensate water on the wall in the steam region, respectively; r is the latent heat of vaporization of the steam in the steam region, kJ/kg.

2.2.1.4. Interface mass transfer. The net rate of condensation at the interface between the steam and water regions of the EB can be calculated by [18].

$$W_{ce} = f\frac{A}{\sqrt{2\pi RT_l}}(P - P^*) \tag{13}$$

where f is an empirical constant; R is the Boltzmann's constant; T_l is the liquid temperature in the inner or outer cylinder of the EB, °C; P^* is the saturation pressure corresponding to T_l, MPa.

2.2.1.5. Electrical conductivity. The relationship between the electrical conductivity and temperature of the liquid in the EB can be given as

$$\sigma = \sigma_0 + \alpha T_l \tag{14}$$

where σ is the electrical conductivity, $\Omega^{-1}\cdot m^{-1}$; α is a coefficient; σ_0 is the electrical conductivity when $T_l = 18$ °C, $\Omega^{-1}\cdot m^{-1}$.

2.2.2. Mathematical model

In this study, a dynamic mathematical model of the EB is developed based on the conservation laws of mass, energy, and volume.

The mass and energy conservation equations for the inner cylinder water region of the EB can be, respectively, given as

$$\frac{dM_{bli}}{dt} = W_{bli,fwi} + \beta W_{bs,bc} + W_{bli,ce} - W_{bli,dwo} - W_{bli,be} \tag{15}$$

$$\frac{d(M_{bli}h_{bli} - P_bV_{bli})}{dt} = W_{bli,fwi}h_{blo} + (\beta W_{bs,bc} + W_{bli,ce})h_{b,f} - W_{bli,dwo}h_{bli} - W_{bli,be}h_{b,g} \tag{16}$$

where M_{bli} is the water mass in the inner cylinder, kg; $W_{bli,fwi}$ is the circulating water flow rate from the inner cylinder to the outer cylinder, which is the flow rate of the circulation pump, kg/s; $W_{bs,bc}$ is the bulk condensation (rain-out) flowrate in the steam region, kg/s; β is the fraction of bulk condensate water falling into the inner cylinder water region, which can be determined approximated by the ratio of the inner cylinder cross-sectional area to the outer cylinder cross-sectional area; $W_{bli,ce}$ is the net rate of condensation flow rate at the interface between the steam and inner cylinder water regions, kg/s; $W_{bli,dwo}$ is the drain water flow rate of the inner cylinder, kg/s; $W_{bli,be}$ is the bulk evaporation (bubble rising) flow rate in the inner cylinder water region, kg/s; h_{bli} and h_{blo} are the specific enthalpies of water in the inner and outer cylinders, respectively, kJ/kg; $h_{b,f}$ and $h_{b,g}$ are the enthalpies of saturated water and steam in the EB, respectively, kJ/kg; P_b is the EB pressure, MPa; V_{bli} is the volume of the inner cylinder water region, m^3.

The mass and energy conservation equations in the outer cylinder of the EB can be, respectively, given as

$$\frac{dM_{blo}}{dt} = W_{blo,fwi} + W_{bli,dwo} + (1-\beta)W_{bs,bc} + W_{blo,ce} + W_{bs,wc} - W_{blo,dwo} - W_{bli,fwi} - W_{blo,be} \tag{17}$$

$$\frac{d(M_{blo}h_{blo} - P_bV_{blo})}{dt} = W_{blo,fwi}h_{blo,fwi} + W_{bli,dwo}h_{bli} + [(1-\beta)W_{bs,bc} + W_{blo,ce} + W_{bs,wc}]h_{b,f} - W_{blo,dwo}h_{blo} - \left(W_{bli,fwi} + W_{blo,be}\right)h_{b,g} \tag{18}$$

where M_{blo} is the water mass in the outer cylinder, kg; $W_{blo,fwi}$ is the feedwater flow rate of the EB, which comes from the deaerator, kg/s; $W_{blo,sc}$ is the net rate of condensation flow rate at the interface between the steam and outer cylinder water regions, kg/s; $W_{bs,wc}$ is the steam condensation flow rate on the wall, kg/s; $W_{blo,dwo}$ is the drain water flow rate of the outer cylinder, kg/s; $W_{blo,be}$ is the bulk evaporation (bubble rising) flow rate in the outer cylinder water region, kg/s; V_{blo} is the volume of the outer cylinder water region, m^3; $h_{blo,fwi}$ is the specific enthalpy of the EB inlet feedwater, kJ/kg.

The mass and energy conservation equations for the steam region of the EB can be, respectively, given as

$$\frac{dM_{bs}}{dt} = W_{bli,be} + W_{blo,be} - W_{bs,bc} - W_{bli,ce} - W_{blo,ce} - W_{bs,wc} - W_{b,so} \tag{19}$$

$$\frac{d(M_{bs}h_{bs} - P_bV_{bs})}{dt} = (W_{bl,be} + W_{blo,be})h_{b,g} - (W_{bs,bc} + W_{bli,ce} + W_{blo,ce} + W_{bs,wc})h_{b,f} - W_{b,so}h_{bs} \tag{20}$$

where M_{bs} is the mass of steam in the EB, kg; $W_{b,so}$ is the outlet steam flow rate of the EB, kg/s; h_{bs} is the specific enthalpy of steam in the EB, kJ/kg; V_{bs} is the volume of the steam region, m^3.

The volume conservation equation of the EB can be expressed as

$$\frac{dV_b}{dt} = \frac{d(M_{bs}v_{bs} + M_{bli}v_{bli} + M_{blo}v_{blo})}{dt} = 0 \tag{21}$$

where V_b is the total volume of the EB, m^3; v_{bs}, v_{li}, and v_{lo} are the specific volumes of the steam or water in the steam, inner cylinder water, and outer cylinder water regions of the EB, respectively, m^3/kg.

The mass and energy differential terms in Eqs. (15)-(20) can be expanded, respectively, as

$$\frac{dM}{dt} = \frac{d(\rho V)}{dt} = \rho\frac{dV}{dt} + V\frac{d\rho}{dt} = \rho\frac{dV}{dt} + V\left(\frac{\partial\rho}{\partial h}\frac{dh}{dt} + \frac{\partial\rho}{\partial P}\frac{dP}{dt}\right) \tag{22}$$

$$\frac{d(Mh - PV)}{dt} = h\frac{dM}{dt} + M\frac{dh}{dt} - 10^3V\frac{dP}{dt} - 10^3P\frac{dV}{dt} \tag{23}$$

Substitution of Eqs. (22) and (23) into Eqs. (15)-(20) yields

$$
\begin{cases}
\rho_{bli}\dfrac{dV_{bli}}{dt}+V_{bli}\left(\dfrac{\partial\rho_{bli}}{\partial h_{bli}}\dfrac{dh_{bli}}{dt}+\dfrac{\partial\rho_{bli}}{\partial P_b}\dfrac{dP_b}{dt}\right)=W_{bli\_fwi}+\beta W_{bs,bc}+W_{bli,ce}-W_{bli,dwo}-W_{bli\_be}\\
-10^3P_b\dfrac{dV_{bli}}{dt}+M_{bli}\dfrac{dh_{bli}}{dt}-10^3V_{bli}\dfrac{dP_b}{dt}=W_{bli,fwi}h_{blo}+(\beta W_{bs,bc}+W_{bli,ce})h_{b,f}-W_{bli,dwo}h_{bli}-W_{bli,be}h_{b,g}-\left(W_{bli,fwi}+\beta W_{bs,bc}+W_{bli,ce}-W_{bli,dwo}-W_{bli,be}\right)h_{bli}\\
\rho_{blo}\dfrac{dV_{blo}}{dt}+V_{blo}\left(\dfrac{\partial\rho_{blo}}{\partial h_{blo}}\dfrac{dh_{blo}}{dt}+\dfrac{\partial\rho_{blo}}{\partial P_b}\dfrac{dP_b}{dt}\right)=W_{blo,fwi}+W_{bli,dwo}+(1-\beta)W_{bs,bc}+W_{blo,ce}+W_{bs,wc}-W_{blo,dwo}-W_{bli,fwi}-W_{blo,be}\\
-10^3P_b\dfrac{dV_{blo}}{dt}+M_{blo}\dfrac{dh_{blo}}{dt}-10^3V_{blo}\dfrac{dP_b}{dt}=W_{blo,fwi}h_{blo,fwi}+W_{bli,dwo}h_{bli}+\left[(1-\beta)W_{bs,bc}+W_{blo,ce}+W_{bs,wc}\right]h_{b,f}-W_{blo,dwo}h_{blo,dwo}-\left(W_{bli,fwi}+W_{blo,be}\right)h_{b,g}\\
\quad-\left[W_{blo,fwi}+W_{bli,dwo}+(1-\beta)W_{bs,bc}+W_{blo,ce}+W_{bs,wc}-W_{blo,dwo}-W_{bli,fwi}-W_{blo,be}\right]h_{blo}\\
-\rho_{bs}\left(\dfrac{dV_{bli}}{dt}+\dfrac{dV_{blo}}{dt}\right)+V_{bs}\left(\dfrac{\partial\rho_{bs}}{\partial h_{bs}}\dfrac{dh_{bs}}{dt}+\dfrac{\partial\rho_{bs}}{\partial P_b}\dfrac{dP_b}{dt}\right)=W_{bli,be}+W_{blo,be}-W_{bs,bc}-W_{bli,ce}-W_{blo,ce}-W_{bs,wc}-W_{b,so}\\
10^3P_b\left(\dfrac{dV_{bli}}{dt}+\dfrac{dV_{blo}}{dt}\right)+M_{bs}\dfrac{dh_{bs}}{dt}-10^3V_{bs}\dfrac{dP_b}{dt}=(W_{bli,be}+W_{blo,be}+W_{blo,se})h_{b,g}-(W_{bs,bc}+W_{bli,ce}+W_{blo,ce}+W_{bs,wc})h_{b,f}-W_{b,so}h_{bs}\\
\quad-(W_{bli,be}+W_{blo,be}-W_{bs,bc}-W_{bli,ce}-W_{blo,ce}-W_{bs,wc}-W_{b,so})h_v
\end{cases}
\tag{24}
$$

where ρ_{bs}, ρ_{bli}, and ρ_{blo} are the densities of steam or water in the steam, inner cylinder water, and outer cylinder water regions, respectively, kg/m^3.

2.3. Deaerator model

The deaerator is an important equipment in the EB system, which is a hybrid heat exchanger. It plays an important role in removing oxygen from the feed water of the EB and preventing corrosion of heat pipes. At the same time, it is also an important water storage vessel, and its level adjustment capability ensures a stable flow of feedwater into the EB. The deaerator in this study is a built-in thermal deaerator, in which the incoming heating steam heats the feedwater of the EB to make its temperature close to the saturation temperature and remove oxygen. The deaerator is mainly composed of a deaerating head and a water tank, as shown in Fig. 2.

Based on the structure and operating characteristics of the deaerator, this study establishes a dynamic mathematical model of the deaerator based on the conservations of mass, energy, and volume.

The energy conservation equation of the deaerator can be given as

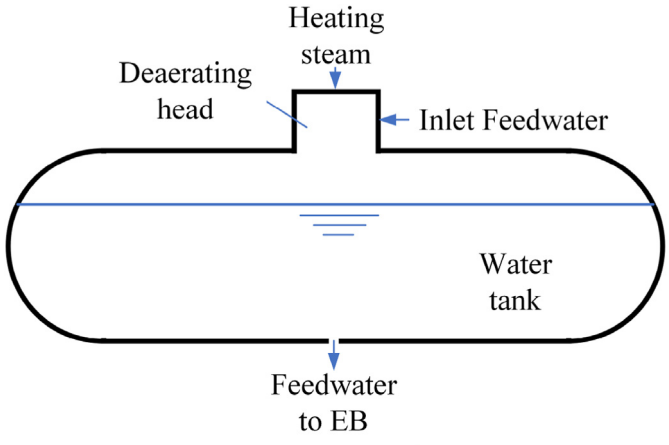

Fig. 2. Schematic of the deaerator.

$$
\frac{d\left(V_{d,f}\rho_{d,f}+V_{d,g}\rho_{d,g}+V_{d,c}\rho_{d,c}\right)}{dt}=W_{d,si}+W_{d,fwi}-W_{d,fwo} \tag{25}
$$

where $V_{d,g}$, $V_{d,f}$, and $V_{d,c}$ are the volumes of the steam, saturated water, and subcooled water in the deaerator, respectively, m^3; $\rho_{d,f}$ and $\rho_{d,g}$ are the densities of the saturatue water and steam in the deaerator, respectively, kg/m^3; $\rho_{d,c}$ is the density of the subcooled water in the deaerator, kg/m^3; $W_{d,si}$ is the inlet heating steam flow rate of the deaerator, kg/s; $W_{d,fwi}$ is the inlet feedwater flow rate of the deaerator, kg/s; $W_{d,fwo}$ is the outlet feedwater flow rate of the deaerator, and $W_{d,fwo}=W_{blo,fwi}$, kg/s.

The energy conservation equation of the deaerator can be expressed as

$$
\frac{d\left(V_{d,f}\rho_{d,f}h_{d,f}+V_{d,g}\rho_{d,g}h_{d,g}+V_{d,c}\rho_{d,c}h_{d,c}+\mu_{d,m}T_{d,m}\right)}{dt}=W_{d,si}h_{d,si}+W_{d,fwi}h_{d,fwi}-W_{d,fwo}h_{d,fwo} \tag{26}
$$

where $h_{d,f}$, $h_{d,g}$, and $h_{d,c}$ are the specific enthalpies of the saturated water, steam, and subcoolded water in the deaerator, kJ/kg; $\mu_{d,m}$ is the total effective heat capacity of the deaerator wall metal, kJ/°C; $T_{d,m}$ is the wall metal temperature, °C, the rate of change of which is approximately the same as that of the steam saturation temperature; $h_{d,si}$, $h_{d,fwi}$, and $h_{d,fwo}$ are the specific enthalpies of the deaerator heating steam, inlet feedwater, and outlet feedwater, respectively, kJ/kg.

The volume conservation equation of the deaerator can be expressed as

$$
V_{d,f}+V_{d,g}+V_{d,c}=V_d \tag{27}
$$

where V_d is the total volume of deaerator, and $dV_d/dt=0$, m^3.

From Eqs. (25) and (26), the rate of change of water volume in the deaerator can be obtained as

$$
\frac{d\left(V_{d,f}+V_{d,c}\right)}{dt}=\frac{W_{d,si}+W_{d,fwi}-W_{d,fwo}-\left(V_{d,f}\frac{d\rho_{d,f}}{dP_d}+V_{d,g}\frac{d\rho_{d,g}}{dP_d}\right)\frac{dP_d}{dt}}{\rho_{d,f}-\rho_{d,g}} \tag{28}
$$

Substatution of Eqs. (27) and (28) into Eq. (26) yields

$$\frac{dP_d}{dt}=\frac{W_{d,si}h_{d,si}+W_{d,fwi}h_{d,fwi}-W_{d,fwo}h_{d,fwo}-\left(W_{d,si}+W_{d,fwi}-W_{d,fwo}\right)\frac{\rho_{d,f}h_{d,f}-\rho_{d,g}h_{d,g}}{\rho_{d,f}-\rho_{d,g}}}{V_{d,f}\frac{d(\rho_{d,f}h_{d,f})}{dP}+V_{d,g}\frac{d(\rho_{d,g}h_{d,g})}{dP}+M_{d,m}\frac{dt_{d,m}}{dP}-\frac{\rho_{d,f}h_{d,f}-\rho_{d,g}h_{d,g}}{\rho_{d,f}-\rho_{d,g}}\left(V_{d,f}\frac{d\rho_{d,f}}{dP_d}+V_2\frac{d\rho_{d,g}}{dP_d}\right)} \tag{29}$$

According to the geometry of the deaerator water tank, the relationship between the water volume and water level of the deaerator can be given by

$$V_{d,f}+V_{d,c}=\begin{cases}\left[\arccos\left(\frac{R_d-H_{d,w}}{R_d}\right)R_d^2-(R_d-H_w)\sqrt{R_d^2-(R_d-H_{d,w})^2}\right](L_d-2R_d)\\ \quad+\frac{1}{3}\pi(3R_d-H_{d,w})H_{d,w}^2, \quad if\ \ V_{d,f}+V_{d,c}\le 0.5V_d\\ \left[\left(\pi-\arccos\left(\frac{H_{d,w}-R_d}{R_d}\right)\right)R_d^2-(H_w-R_d)\sqrt{R^2-(R_d-H_{d,w})^2}\right](L_d-2R_d)\\ \quad+\frac{4}{3}\pi R_d^3-\frac{1}{3}\pi(R_d+H_{d,w})(2R_d-H_{d,w})^2, \quad otherwise\end{cases} \tag{30}$$

where $H_{d,w}$ is the deaerator water level, m; R_d and L_d are the radius and length of the deaerator water tank, respectively, m; V_d is the volume of the deaerator water tank, m^3.

The rate of change of $V_{d,c}$ can be calculated by

$$\frac{dV_{d,c}}{dt}=\frac{A_{d,c}}{\rho_{d,f}g}\frac{dP_d}{dt} \tag{31}$$

$$A_{d,c}=\pi\left[R_d^2-(R_d-H_{d,w})^2\right]+2(L_d-2R_d)\sqrt{R_d^2-(R_d-H_{d,w})^2} \tag{32}$$

where $A_{d,c}$ is the cross-sectional aera of the deaerator water tank at the corresponding vaporization depth, m^2.

Assuming that the deaerator is in a steady state when its pressure drops, the water temperature is approximately equal to the saturation temperature. Then the water within the water surface to a depth of $\frac{|dP_d|}{\rho_{d,f}g}$ is partially vaporized owing to the temperature being higher than the saturation temperature at the corresponding pressure, giving off heat to reach saturation. Because of the influence of the static pressure of the water column, the water below this depth is still in a subcooled state, although its temperature is higher than the saturation temperature at the steam pressure of the deaerator. As the pressure continues to fall, the depth of the water that can be vaporized gradually increases, which is called the vaporization depth. And the rate of change of the unsaturated water can be determined by $\frac{A_{d,c}}{\rho_{d,f}g}\left|\frac{dP_d}{dt}\right|$. Once the depth of vaporization is the same as the water level in the deaerator, all the water is saturated at the corresponding pressure as the pressure continues to fall.

Approaching the bottom of the deaerator water tank, where the horizontal cross-sectional area is smaller and the feedwater flow is accelerated, the forced flow caused by the outlet feedwater pump has an influence on the variation of the vaporization depth. Then, during the pressure drop transients of the deaerator, the following relationship much be judged.

$$\left|\frac{dP_d}{dt}\right|\frac{1}{\rho_{d,f}g}<\frac{W_{d,fwo}}{\rho_{d,f}A_{d,c}} \tag{33}$$

When the above equation is satisfied, the vaporization depth gradually increases, and we have $dV_{d,c}/dt=0$. Otherwise, the rate of change of $V_{d,c}$ should be calculated by Eq. (31). This is because when the water at the vaporization depth falls too quickly, the pressure head of the water column above it also increases rapidly. If the absolute value of the pressure change is less than the change in the pressure head of the water column, the absolute pressure of this part of water increases. Its temperature is even lower than the saturation temperature at the corresponding pressure and cannot release heat quickly. In this case, the depth of vaporization no longer increases.

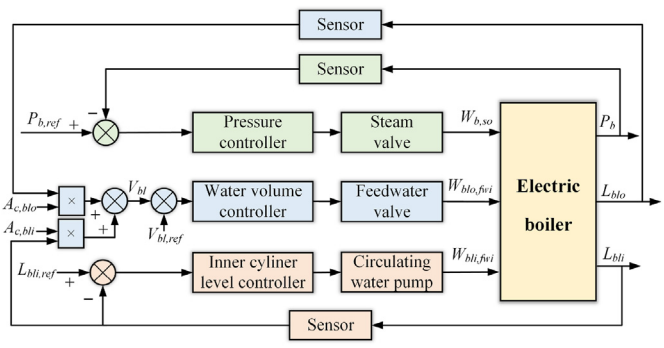

Fig. 3. Block diagram of the EB pressure, power, and water volume control systems.

3. Operation characteristics and control systems of the EB system

3.1. Operation characteristics

The operation of the EB system has to be adapted to the requirements of the entire NPP for steam supply. The EB of the HTR-PM plant has three operation modes: normal operation, hot standby, and cold standby.

3.1.1. Normal operation

During normal operations, the output steam flow rate of the EB is between the minimum flow rate and the rated flow rate. In this condition, the demineralized water enters the deaerator through a feedwater regulating valve that is used to adjust the deaerator water level, and the inlet heating steam from the EB is used for heating the feedwater and deaeration. Before the heating steam enters the deaerator, it passes through a control valve to maintain the deaerator pressure. The feedwater from the deaerator is first pressurized by a feedwater pump, and then a feedwater valve regulates the feedwater flow rate to maintain a constant amount of water volume in the inner and outer cylinders of the EB.

The water from the outer cylinder of the EB is continuously injected into the inner cylinder through the circulation pump, which is heated by the three-phase electrodes to generate steam. The water level in the inner cylinder is controlled by the regulating valve deployed at the outlet header of the circulation pump, which determines the EB load, which is controlled by the circulation pump.

A steam control valve is deployed at the top of the EB to regulate its outlet steam flow rate. Part of the steam enters the deaerator as heating steam, and the remaining steam is sent to the auxiliary steam header in the secondary-loop of the plant. During cold or hot start-up of the plant, part of the steam generated by the EB will be further heated by a superheater before sent to the turbine shaft seal system.

The EB of the HTR-PM plant can continuously produce up to 42 t/h of steam. The rated steam parameters before the EB outlet control valve are 1.6 MPa and 204 °C. The cold and hot start-up times of the EB are 59min and 5min, respectively. The rated output of the deaerator is 92 t/h and the maximum output is 102 t/h. The rated operating pressure of the deaerator is 0.12 MPa, and the rated temperature is 105 °C. The amount of steam required for thermal deaeration of the deaerator is 6.3 t/h. Under normal operating conditions, the deaerator level is maintained at 1540 mm by regulating the inlet feewater flowrate.

3.1.2. Hot standby

The hot standby operation is a type of standby mode, which is designed to shorten the EB start-up time. In this condition, the EB temperature is maintained by two 50 kW electric heaters (one for use and the other for standby) deployed in the outer cylinder. And the deaerator temperature is also maintained by two 50 kW electric heaters with one for use and the other for backup.

In hot standby operations, the feedwater and circulation pumps of the EB are in standby states, and the control logic of the corresponding pumps and control valves are in “automatic mode”. The feedwater pump and valve of the EB maintains its outer cylinder water level at a specific position between the maximum and minimum water level setpints. While the inner cylinder water level is zero under the current design. For the deaerator, its water level is maintained by regulating its inlet feedwater valve.

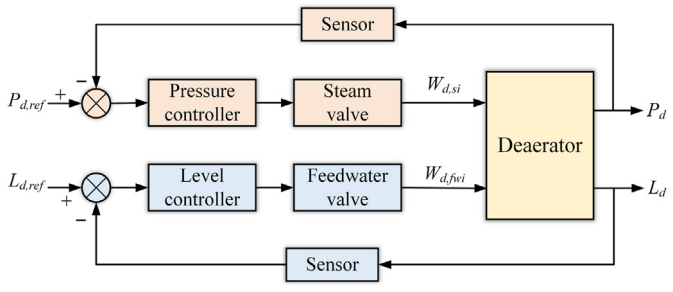

Fig. 4. Block diagram of the deaerator pressure and water level control systems.

3.1.3. Cold standby

The cold standby operation is another type of standby mode. In cold standby condition, the equipment is maintained in wet status, and the EB and deaerator are completely filled with cold water. The water level in the EB is maintained at the steam outlet elevation.

3.2. Control systems

3.2.1. EB control systems

This study only focuses on the operating and control characteristics of the EB from the hot standby to normal operations, and the control systems involved are mainly the pressure control system, inner cylinder level control system, and water volume control system, as shown in Fig. 3. Here, L_{bli} and L_{blo} are the water levels of the EB inner and outer cylinders, respectively, m; $A_{c,bli}$ and $A_{c,blo}$ are the cross-sectional areas of the EB inner and outer cylinders, respectively, m; $P_{b,ref}$, $L_{bli,ref}$, and $V_{bl,ref}$ are the reference values of P_b, L_{bli}, and V_{bl}; V_{bl} is the total water volume in the EB, m^3.

The pressure control system is designed to maintain the EB pressure at its setpoint value, which is 1.6 MPa for the HTR-PM plant, by regulating the steam control valve of the EB. During the transition from hot standby to normal operations, the steam valve is closed until the steam pressure rises to the setpoint value. After that, the steam valve opening is adjusted smaller or larger when the steam pressure drops below or rise above the stepoint value.

The power of the EB three-phase electrodes is linearly related to its immersion depth inside the inner cylinder. Therefore, the output power of the EB can be maintained at the setpoint value by regulating the inner cylinder water level which increases linearly with the power. When the inner cylinder water level is lower (higher) than the setpoint value, the circulating water pump and valve will be adjusted to increase (decrease) the circulating water flowrate injected to the inner cylinder from the outer cylinder of the EB.

The water volume controller is designed to maintain a constant water volume in the inner and outer cylinders of the EB. The feedwater valve of the EB is adjusted according to the controller output to achieve this control objective. When the water volume in the EB drops below the setpoint value owing to excessive steam production, etc., the feedwater pump will be adjusted to increase the feedwater flow rate from the deaerator to the EB.

The pressure, inner cylinder level, and water volume controllers were all designed as PI controllers, which were determined based on the PID tuner in MATLAB/Simulink [21] as $50.1+\frac{0.49}{s}$, $102.9+\frac{0.95}{s}$, $20.3+\frac{0.15}{s}$, respectively.

3.2.2. Deaerator control systems

During the transition from hot standby to normal operating conditions in the EB, the pressure and water level of the supporting deaerator need to be controlled, as presented in Fig. 4.

The deaerator pressure are controlled at a constant setpoint value, which is 0.12 MPa to maintain the EB feedwater temperature at ~105 °C in this study, by the deaerator pressure controller. It

controls the flowrate of the heating steam fed into the deaerator by adjusting the inlet steam valve opening. In this way, the feedwater quality of the EB can be guaranteed.

The level controller maintains the deaerator water level at a constant setpoint value which is 1540 mm in this study during its normal operations. When the water level in the deaerator is too high (>1690 mm), a high level alarm will be issued to close the feedwater control valve. When the water level in the deaerator is too low (<550 mm), a low level alarm will be issued to close the feed water pump of the EB and the deaerator backup electric heater. If the deaerator water level reaches the preset high limit (1640 mm), the deaerator relief valve opens, which will close when the water level falls below 1620 mm.

The pressure and level controllers were all designed as PI controllers, which were also determined based on the PID tuner in MATLAB/Simulink [21] as $500.5 + \frac{9.8}{s}$ and $249.6 + \frac{2.2}{s}$, respectively.

4. Optimization strategies for hot standby operations of EB system

During normal operations of the HTR-PM NPP, the EB system is always in hot standby status. However, the current hot standby operation suffers from the following problems. First, it cannot provide qualified steam in a short period of time when the NPP starts up. Second, electric heaters are required to compensate for the heat loss of the EB and deaerator during the hot standby operation, which consumes a lot of electric power and does not meet the economic requirements of the NPP. Moreover, the initial water level of the inner cylinder is zero. Thus, it is necessary to inject water from the outer cylinder to the inner cylinder through the circulation pump first when transforming to normal operations. After the water level of the inner cylinder rises to the start-up level, the three-phase electrodes can be turned on to heat the water in the inner cylinder, resulting in a long transient time. Finally, the EB system needs to run for a long time during the test run, start up, and shut down operations of the NPP. And the current hot standby operation does not consider the backup of superheated steam for the turbine shaft seal system.

To solve the above problems, this study seeks the optimization of the EB hot standby operation strategy in the following aspects. On the one hand, to improve the transition speed of the EB from the hot standby to normal operations, the inner cylinder water level of the EB during the hot standby operation can be changed from zero level to the start-up level which is 600 mm. This can save the time required to supply water from the outer cylinder to the inner cylinder when transiting from the hot standby to normal operations. On the other hand, to reduce electric power consumption, the heating method of the EB and deaerator can be changed from electric heating to steam heating during the hot standby operation. For the EB, part of steam can be extracted from the main steam system of the plant through the EB outlet steam pipe into its outer cylinder to compensate for the heat loss to the external

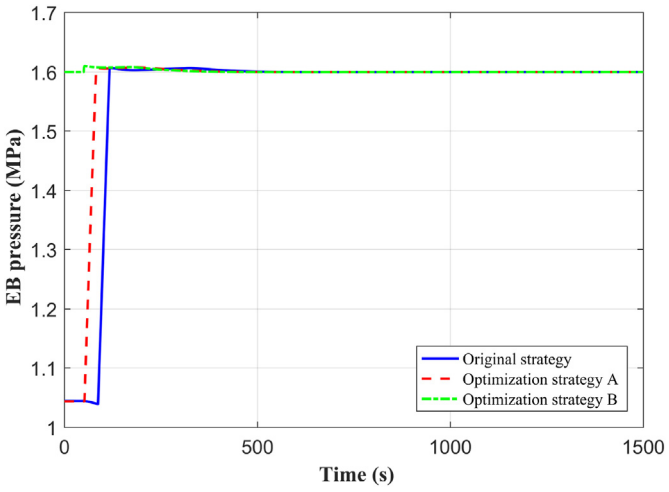

Fig. 6. Dynamic responses of the EB pressure during transition from hot standby to normal operations under different operation strategies.

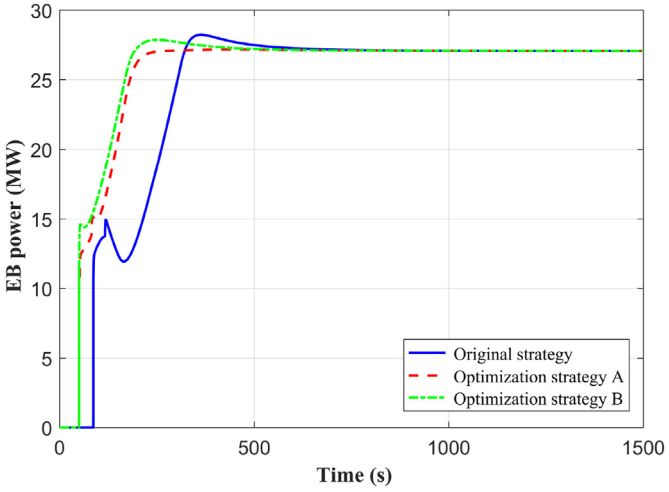

Fig. 7. Dynamic responses of the EB power during transition from hot standby to normal operations under different operation strategies.

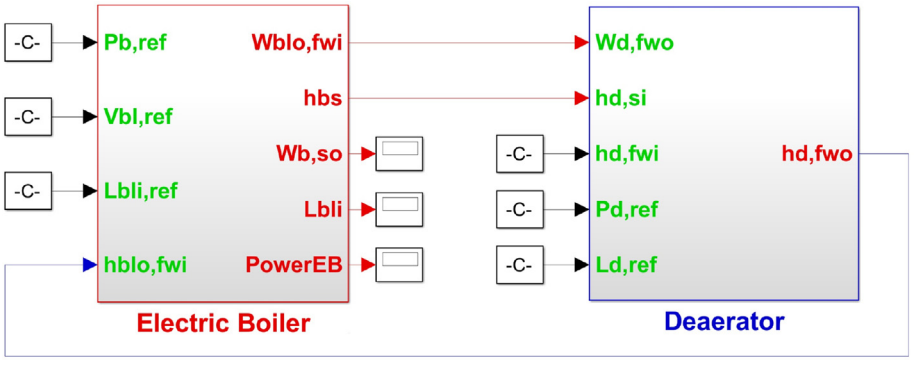

Fig. 5. Block diagram of the dynamic simulation platform for the EB system using Simulink.

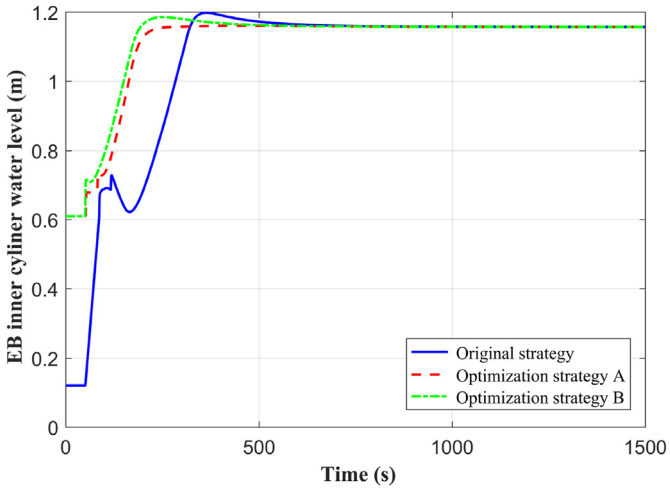

Fig. 8. Dynamic responses of the EB inner cylinder water level during transition from hot standby to normal operations under different operation strategies.

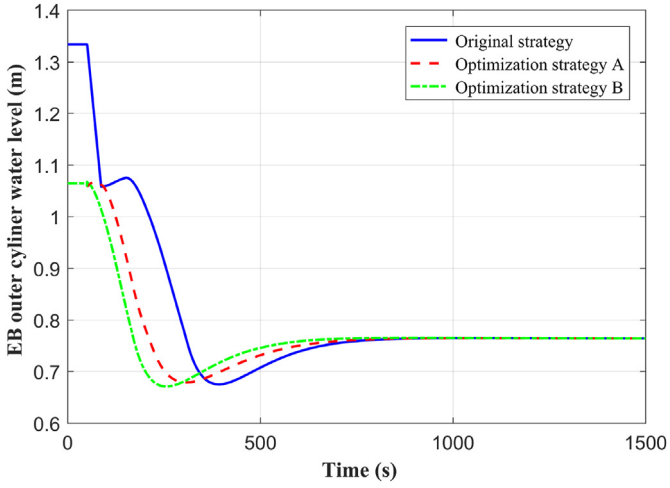

Fig. 9. Dynamic responses of the EB outer cylinder water level during transition from hot standby to normal operations under different operation strategies.

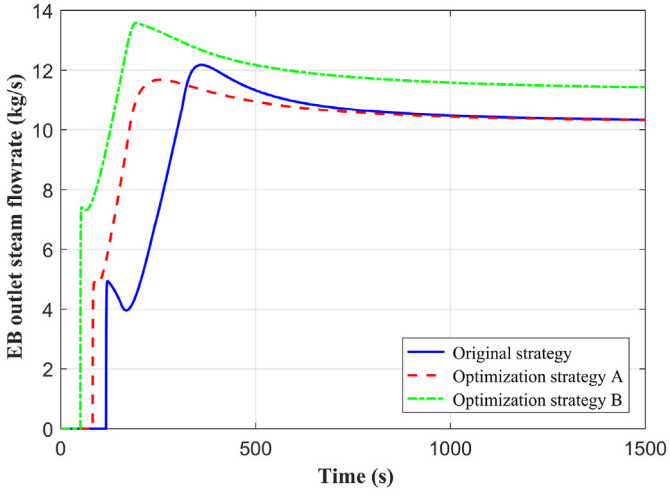

Fig. 10. Dynamic responses of the EB outlet steam flowrate during transition from hot standby to normal operations under different operation strategies.

environment. At the same time, part of steam can be extracted from the main steam system as the heating steam of the deaerator, which replaces the electric heaters of the deaerator during the hot standby operation to compensate its heat loss to the external environment. With these improvements, the electric heating of the EB and deaerator during the hot standby operating can be eliminated, which can greatly reduce the electric power consumption. Based on the above analysis, optimization strategies for the hot standby operation of the EB and deaerator are proposed.

The hot standby operations of the EB under the original strategy and two optimization strategies are illustrated as follows.

(1) Original strategy for the EB. The electric heaters are used to compensate for the heat loss in the EB in the hot standby operation, and the initial water level of the inner cylinder is zero.
(2) Optimization strategy A for the EB. The electric heaters are used to compensate for the EB heat loss in the hot standby operation, and the initial water level of the inner cylinder is the start-up level.
(3) Optimization strategy B for the EB. Part of steam is extracted from the main steam system of the plant to compensate for the EB heat loss in the hot standby operation, and the initial water level of the inner cylinder is the start-up level.

The hot standby operations of the deaerator under the original strategy and the proposed optimization strategy are illustrated as follows.

(1) Original strategy for the deaerator. The electric heaters are used to compensate for the heat loss in the deaerator during the hot standby operation.
(2) Optimization strategy for the deaerator. Part of steam is extracted from the main steam system of the plant to compensate for the deaerator heat loss during the hot standby operation.

These optimization strategies are verified through numerical simulations, and the simulation results and discussion are given in the following Section 5.

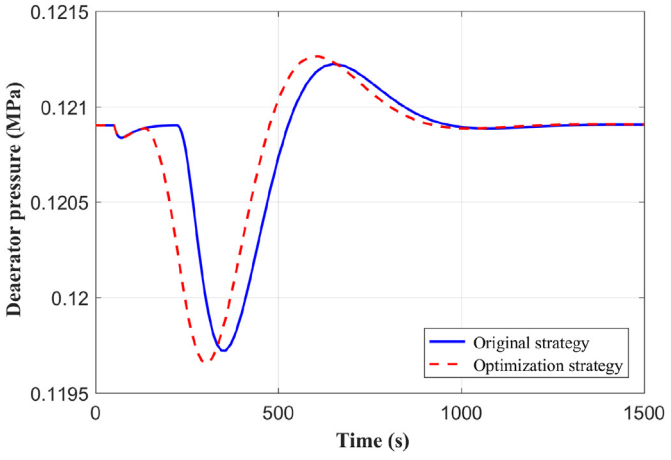

Fig. 11. Dynamic responses of the deaerator pressure during transition from hot standby to normal operations under different operation strategies.

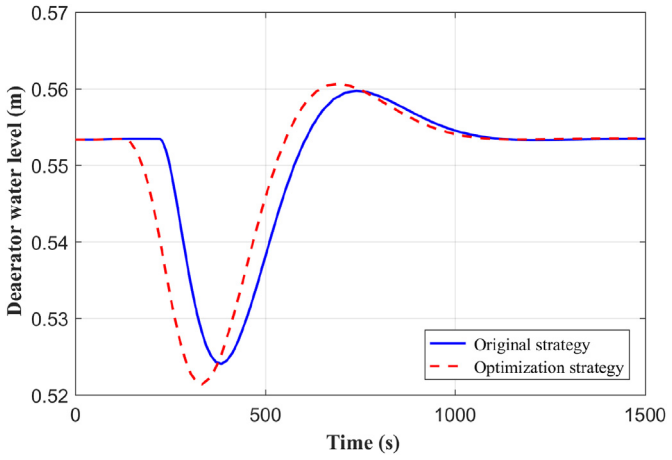

Fig. 12. Dynamic responses of the deaerator water level during transition from hot standby to normal operations under different operation strategies.

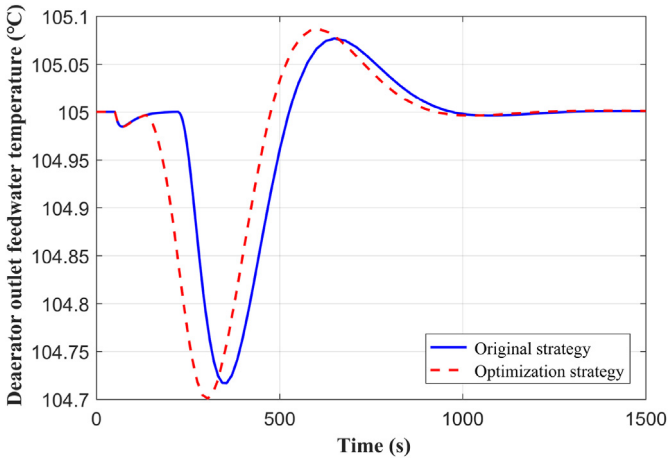

Fig. 13. Dynamic responses of the deaerator outlet feedwater temperature during transition from hot standby to normal operations under different operation strategies.

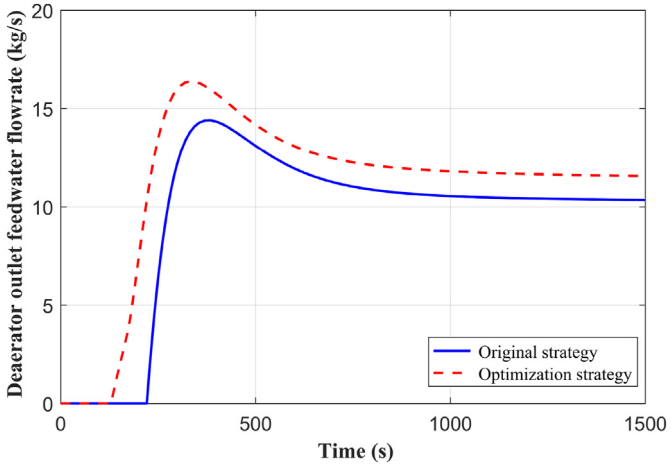

Fig. 14. Dynamic responses of the deaerator outlet feedwater flow rate during transition from hot standby to normal operations under different operation strategies.

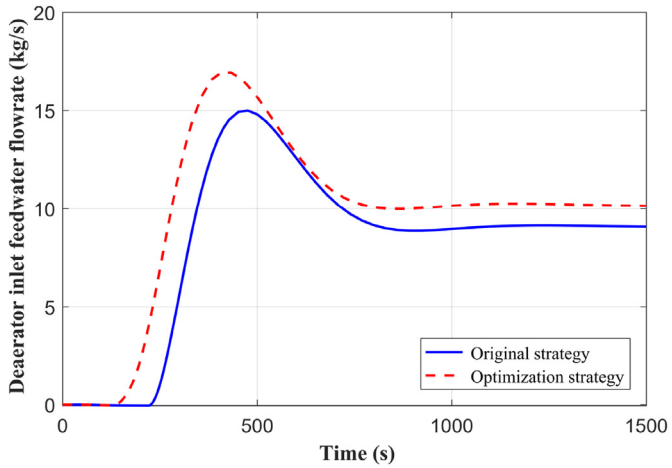

Fig. 15. Dynamic responses of the deaerator inlet feedwater flow rate during transition from hot standby to normal operations under different operation strategies.

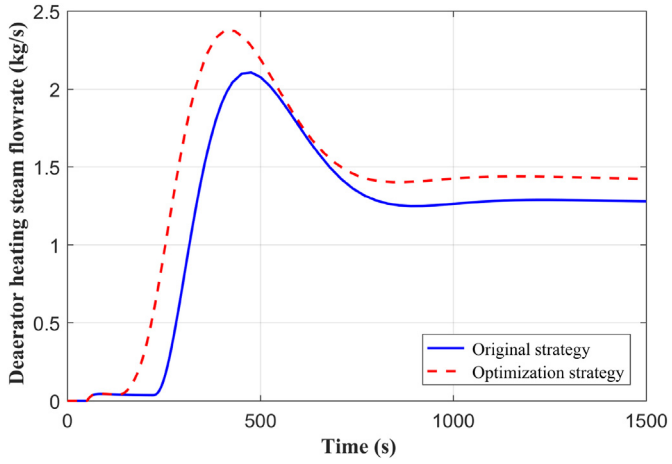

Fig. 16. Dynamic responses of the deaerator heating steam flow rate during transition from hot standby to normal operations under different operation strategies.

5. Results and discussion

The feasibility and advancement of the proposed optimization strategies were verified through dynamic simulations. A dynamic simulation platform of the EB system was developed in MATLAB/Simulink with implementation of the established EB and deaerator models and control systems as well as the proposed optimization strategies, as shown in Fig. 5. Here, PowerEB denotes the EB power. The ode15s Solver in Simulink is employed to solve the dynamic models of the EB and deaerator during transient simulations.

5.1. Optimization results of the EB

Under the original strategy and proposed two optimization strategies for the EB, dynamic responses of the EB key parameters during the transition transient from the hot standby to normal operations are shown in Figs. 6–10.

From Figs. 6–10, the following analysis results can be drawn for the EB.

(1) According to Figs. 7 and 8, the transient times for the electrode power to reach the rated value are 321.42s, 241.23s, and 194.19s for the three strategies of the EB, respectively. This indicates that when the inner cylinder level is the start-up level at the hot standby operation, the inner cylinder water level and electrode power of the EB reach the normal operating values much faster than those when the initial inner cylinder water level is zero.
(2) Compared with the original strategy, the proposed optimization strategies do not change the equilibrium values of the pressure, power, and inner and outer cylinder water levels when the EB reaches normal operating conditions, as shown in Figs. 6–9.
(3) Under the optimization strategy B, the steam is removed from the EB as soon as the transition from the hot standby to normal operations begins, as shown in Fig. 10. This is because the use of steam heating instead of electric heating, so the EB has a certain amount of steam during the hot standby operation, and the pressure can be maintained at the rated value (1.6 MPa). While for the original strategy and the optimization strategy A, the EB pressure is much lower than the rated value during hot standby operations, and a certain amount of steam needs to be accumulated to reach the rated pressure. Therefore, the generated steam is not discharged from the EB for a period of time after the electrodes are turned on, which is equivalent to that the initial electrode power is absorbed by the EB itself. This causes the final steam flow rates under the original strategy and optimization strategy A to be lower than that under the optimization strategy B of the EB. The flow rate differences compensate for the amount of steam needed to increase the EB pressure under the original strategy and optimization strategy A.
(4) The power consumptions during the hot standby operations under the three strategies are, respectively, calculated as follows.
- The electric power consumptions of the EB and circulation pump under the original strategy are 100 kW and 0 kW, respectively. Thus, the total power consumption is 100 kW.
- The rated power of the circulation pump is 15 kW, and the power required for the circulation pump to maintain the inner cylinder at the start-up level is ~40% of its rated power during the hot standby operation. Thus, the power consumption of the circulation pump is ~6 kW, and the total power consumption under the optimization strategy A is the sum of the electric power (100 kW) and the circulation pump power, which is 106 kW.
- Under the optimization strategy B, the flow rate of the heating steam injected into the EB from the main steam system is 0.0581 kg/s, with the temperature of 202.4 °C and specific enthalpy of 2795.9 kJ/kg. The thermal heat to power conversion efficiency can be taken as ~40%, then the equivalent power consumption for the heating steam is ~64.95 kW. Therefore, the total power consumption under the optimization strategy B is the sum of the heating power and the circulation pump power, which is 70.95 kW.

In summary, the transient response of the EB transiting from the hot standby to normal operations under the optimization strategy A is faster than that under the original strategy, with a little increase in the electric power consumption. While for the optimization strategy B, it enables the EB to response much faster with less electric power consume during the transition from hot standby to normal operations, compared with the original strategy and the optimization strategy A. Therefore, the optimization strategy B is the optimal operational strategy among the three strategies for the EB.

5.2. Optimization results for the deaerator

Under the original and proposed optimization strategies for the deaerator, dynamic responses of the deaerator key parameters during the transition transient from hot standby to normal operations are shown in Figs. 11–16. During the transition from hot standby to normal operations of the EB, part of the EB outlet steam will be used as heating steam for the deaerator. Thus, the operating scheme of the EB also affects the dynamic responses of the deaerator. For the simulation results of the deaerator under the original and optimization strategies presented in the following figures, the original strategy and optimization strategy B of the EB were adopted, respectively.

From Figs. 11–16, the following analysis results can be drawn.

(1) It can be observed from that, compared with the original strategy, the proposed optimization strategy does not change the equilibrium values of the deaerator pressure, water level, and outlet feedwater temperature when reaching normal operating conditions, as shown in Figs. 11–13.
(2) As illustrated in Section 5.1, to maintain the EB pressure at the setpoint during the transition transient from hot standby to normal operations, the EB outlet steam flow rate under the optimization strategy B is higher than that under the original strategy. Thus, to keep the EB water volume constant, its feedwater flow rate from the deaerator is increased, resulting in an increase in the deaerator outlet feedwater flow. Therefore, to maintain the deaerator water level and pressure, the inlet feedwater and heating steam flow rates under the optimization strategy are higher than that under the original operating strategy of the deaerator, as illustrated in Figs. 14–16.
(3) The optimization strategy can increase the dynamic response speed of the deaerator from hot standby to normal operations, with a slightly increase in the overshoots of deaerator pressure, level and outlet temperature.
(4) The power consumptions during the hot standby operations under the original and optimization strategies of the deaerator are, respectively, calculated as follows.
- Under the original strategy, the electric heaters with the power of 100 kW are employed to compensate for the heat loss of the deaerator. Thus, the total power consumption of the deaerator is 100 kW in this case.
- Under the optimization strategy, the flow rate of the heating steam consumed by the deaerator, which is used to replace the electric heaters to compensate for the deaerator heat loss, is 0.0372 kg/s. The temperature and specific enthalpy of the heating steam are 106 °C and 2685.5 kJ/kg, respectively. Thus, taking the thermal heat to power conversion efficiency as ~40%, the equivalent power consumption for the deaerator is ~40 kW.

In summary, the proposed optimization operating strategy enables the deaerator to response much faster and consume less electric power during the transient from hot standby to normal operating conditions compared with the original strategy.

6. Conclusions

To solve the problems of high power consumption and slow response speed of the HTR-PM EB system during hot standby operations, two optimization strategies are proposed in this paper. The first strategy adjusts the inner cylinder water level of the EB during hot standby operations from zero level to the start-up level to reduce the transition time from hot standby to normal

operations. The second strategy replaces the electric heaters of the EB system by the heating steam extracted from the main steam system of the plant to compensate for its heat loss during hot standby operations. The proposed strategies were verified through dynamic simulations based on a control simulation platform of the EB system developed in MATLAB/Simulink. The results indicate that the extracted heating steam can compensate for the heat loss of the EB and deaerator during hot standby operations, reducing the electric power consumptions of the EB and deaerator by approximate 29.05 kW and 60 kW, respectively, compared with those under the original operation strategies. At the same time, the adjustment of the EB inner cylinder water level to the start-up level during hot standby operations can shorten the transition time from hot standby to normal operations by up to 127.23s compared with that under its original operation strategy, speeding up the response speed of the EB system significantly. Therefore, the feasibility and superiority of the proposed optimization strategies can be demonstrated, which are expected to provide a reference for the performance improvement of EB systems in practical engineering.

Declaration of competing interest

The authors declare that they have no known competing financial interests or personal relationships that could have appeared to influence the work reported in this paper.

Acknowledgement

This research is funded by the Xi'an Thermal Power Research Institute Co., Ltd.

References

[1] H. Reutler, G.H. Lohnert, The modular high-temperature reactor, Nucl. Technol. 62 (1) (1983) 22–30.
[2] H. Reutler, G. Lohnert, Advantages of going modular in HTRs, Nucl. Eng. Des. 78 (2) (1984) 129–136.
[3] H. Frewer, W. Keller, R. Pruschek, The modular high-temperature reactor, Nucl. Sci. Eng. 90 (4) (1985) 411–426.
[4] J.E. Kelly, Generation IV International Forum: a decade of progress through international cooperation, Prog. Nucl. Energy 77 (2014) 240–246.
[5] D.Z. Wang, D.X. Zhong, Y.K. Yu, Present status of research and development for HTR in China, Energy 16 (1) (1991) 159–167.
[6] Z. Zhang, Z.X. Wu, D.Z. Wang, Y.H. Xu, Y.L. Sun, F. Li, Y.J. Dong, Current status and technical description of Chinese 2×250MWth HTR-PM demonstration plant, Nucl. Eng. Des. 239 (7) (2009) 1212–1219.
[7] A.C. Kadak, The status of the US high-temperature gas reactors, Eng. Times 2 (1) (2016) 119–123.
[8] S. Ueta, J. Aihara, K. Sawa, A. Yasuda, M. Honda, N. Furihata, Development of high temperature gas-cooled reactor (HTGR) fuel in Japan, Prog. Nucl. Energy 53 (7) (2011) 788–793.
[9] Z.Y. Zhang, Z.X. Wu, Y.L. Sun, F. Li, Design aspects of the Chinese modular high-temperature gas-cooled reactor HTR-PM, Nucl. Eng. Des. 236 (5) (2006) 485–490.
[10] P.Y. Zhang, Q.Q. Guo, S. Pang, Y.L. Sun, Y. Chen, Experimental research on vertical mechanical performance of embedded through-penetrating steel-concrete composite joint in high-temperature gas-cooled reactor pebble-bed module, Nucl. Eng. Technol. (2022).
[11] W.J. Zeng, Q.F. Jiang, S.M. Du, T.Y. Hui, S. Li, Design of the flexible switching controller for small PWR core power control with the multi-model, Nucl. Eng. Technol. 53 (2021) 851–859.
[12] L. Wang, X.Y. Wei, F.Y. Zhao, X.G. Fu, Modification and analysis of load follow control without boron adjustment for CPR1000, Ann. Nucl. Energy 70 (2014) 317–328.
[13] M.R. Li, W.Z. Chen, J.L. Hao, W.T. Li, Experimental and numerical investigations on effect of reverse flow on transient from forced circulation to natural circulation, Nucl. Eng. Technol. 52 (2020) 1955–1962.
[14] P. Singh, L.K. Singh, Instrumentation and control systems design for nuclear power plant: an interview study with industry practitioners, Nucl. Eng. Technol. 53 (2021) 3694–3703.
[15] J.W. H, J.Q. Yuan, Disturbance observer-based robust backstepping load-following control for MHTGRs with actuator saturation and disturbances, Nucl. Eng. Technol. 53 (2021) 3685–3693.
[16] Z. Dong, Nonlinear adaptive power-level control for modular high temperature gas-cooled reactors, IEEE Trans. Nucl. Sci. 60 (2) (2013) 1332–1345.
[17] D. Jiang, Z. Dong, Dynamic matrix control for thermal power of multi-modular high temperature gas-cooled reactor plants, Energy (198) (2020) 117386.
[18] S.M. Baek, H.C. No, I.Y. Park, A non-equilibrium three-region model for transient analysis of pressurized water reactor pressurizer, Nucl. Technol. 74 (1986) 213–221.
[19] J.F. Wilson, R.J. Grenda, J.F. Patterson, The velocity of rising steam in a bubble two-phase mixture, Trans. Am. Nucl. Soc. 5 (1962) 151.
[20] A. Bejan, A.D. Kraus, Heat Transfer Handbook, John Wiley & Sons, 2003.
[21] Mathworks Inc, Control System Toolbox Documentation, 2016.